Journal of Structural Geology 32 (2010) 1668–1676

Contents lists available at ScienceDirect

Journal of Structural Geology

journal homepage: www.elsevier.com/locate/jsg

Using empirical geological rules to reduce structural uncertainty in seismic interpretation of faults

Brett Freeman [a,*], Peter J. Boult [b], Graham Yielding [a], Sandy Menpes [c]

[a] Badley Geoscience Ltd., North Beck House, North Beck Lane, Hundleby, Lincolnshire PE23 5NB, UK
[b] GINKGO ENPGNG, 57, Seventh Avenue, St. Morris SA 5068, Australia
[c] Palaeosearch, 41 Walker Avenue, Heathfield SA 5153, Australia

ARTICLE INFO

Article history:
Received 3 February 2009
Received in revised form
21 October 2009
Accepted 2 November 2009
Available online 23 November 2009

Keywords:
Normal fault
Displacement
Displacement gradient
Wall-rock strain
Seismic interpretation

ABSTRACT

Good seismic interpretation of faults should include a workflow that checks the interpretation against known structural properties of fault systems. Estimates of wall-rock strains provide one objective means for discriminating between correct and incorrect structural interpretations of 2D and 3D seismic data – implied wall-rock strain should be below a geologically plausible maximum. We call this the strain minimisation approach. Drawing on the large body of published data for strike dimension and maximum displacement for faults we suggest a realistic upper limit of wall-rock shear strain of 0.05, and 0.1 for maximum longitudinal strain when measured in the displacement direction. Small-scale variation of fault wall-rock strain also adheres to this rule, except in specific areas of strain localisation such as relay zones. As a case study we review an existing structural interpretation of 2D seismic surveys. Mapping of shear and longitudinal strain on the fault planes show values commonly greater than 0.05 and 0.1 respectively. Thus the model is deemed inadmissible. We then reinterpreted the area in an iterative manner using the strain minimisation approach. By using regions of implied high wall-rock strain as an indicator of high uncertainty in the interpretation, we were able to break out two self-consistent fault sets, each of which had geologically plausible wall-rock strains, where previously there had only been one fault set with highly implausible wall-rock strains.

1. Introduction

It has been established for more than twenty years that the displacement on geological fault surfaces varies in a smooth, continuous and consistent manner. Rippon (1985) and Barnett et al. (1987) first demonstrated this for isolated normal faults from the English coalfields. They used precise survey data from coal mine plans to measure the throw (vertical component of dip separation) for a number of coal seams at varying spatial locations. When the throw values were plotted on a strike projection of the fault surface, the contours of throw were concentric and sub-parallel, with a maximum throw close to the centre of the fault surface. Moreover the boundary, or tip, of the fault surface was approximately elliptical. These important observations have stimulated an enormous amount of research into the form and scaling relationships of displacement distributions, the quantitative systematics of fault geometry and speculation on fault growth mechanisms. The simplicity of the observations implies both a consistency and a limit to the strain in the wall rocks. Barnett et al. (1987), Bouvier et al. (1989) (normal faults) and then Chapman and Meneilly (1991) (reactivated normal fault with net reverse displacement) demonstrated similar patterns from seismic interpretation. Although the precision of the structural information from seismic data is considerably poorer than the surveyed data of Rippon (1985), these early examples of displacement distributions are also characteristically continuous and smooth.

A priori knowledge of the shape/form of the displacement distribution and its gradients can be useful as an aid to seismic interpretation. Barnett et al. (1987) suggested that it could serve both as a quality control metric and a means to predict quantitatively the location of lithological layers (horizons) and faults where data is limited. In other words it can be used to manage interpretation uncertainty. In faulted reservoirs, structural uncertainty arises from two major sources of error: the systematic error of the seismic method, and the human error of the interpreter. For good quality 3D seismic data the order of error in lateral positioning of structures is approximately the same as the error in the vertical dimension and both are dominantly systematic. However, when the spacing between fault traces from line samples (e.g. seismic lines) is closer than the spacing between the line samples

* Corresponding author. Tel.: +44 (0) 1754 890390; fax: +44 (0) 1790 753527.
E-mail address: brett@badleys.co.uk (B. Freeman).

0191-8141/$ – see front matter © 2009 Elsevier Ltd. All rights reserved.
doi:10.1016/j.jsg.2009.11.001

themselves, the lateral correlation of faults is equivocal (e.g. Freeman et al., 1990). So for 2D seismic data, reconnaissance mapping, poor quality 3D seismic data and for small faults in 3D seismic data, the pattern of faulting becomes a serious interpretive issue. The balance of the error, or uncertainty, is then strongly one-sided and the effects of systematic errors become secondary to those inherent in the interpreter's "model". Freeman et al. (1990) introduced a methodology that used displacement patterns to distinguish likely fault plane correlations from possible and impossible correlations. In a similar vein, Needham et al. (1996) showed how this kind of analysis was valuable for validating three-dimensional structural models. Traditionally the analytical part of the process has taken the form of visual inspection of the throw contours. If the resulting pattern is smooth and continuous, the fault may be judged as a valid interpretation, otherwise the correlation is deemed to be suspect. Although ostensibly objective, the effectiveness of the above approach is dependent on the skill or experience of the interpreter in being able to identify bad contour patterns. We know of no published work that actually quantifies what constitutes either a good or a bad contour pattern. In this paper we suggest that the above basic validation procedure can be improved by (1) quantifying the strains that are implied by the contour patterns and (2) setting out reasonable limits for the magnitudes of these strains.

We show that there is a simple relationship between strain and the displacement gradient. Drawing from a large database of published information on the shapes of displacement profiles and the scaling relationship between displacement and fault dimension, we can suggest reasonable limits on the amount of strain that is admissible in the walls of a fault. Implied strains that exceed these empirical limits indicate flaws in the structural model. The resulting strategy for interpretation leads to a structural model that minimizes the strain attributable to faulting.

As an example we show how an analysis of a 2D seismic interpretation from South Australia consistently implies erratic and unrealistically large strains. An iterative structural reinterpretation using our minimum strain approach provides a solution that is geologically more feasible.

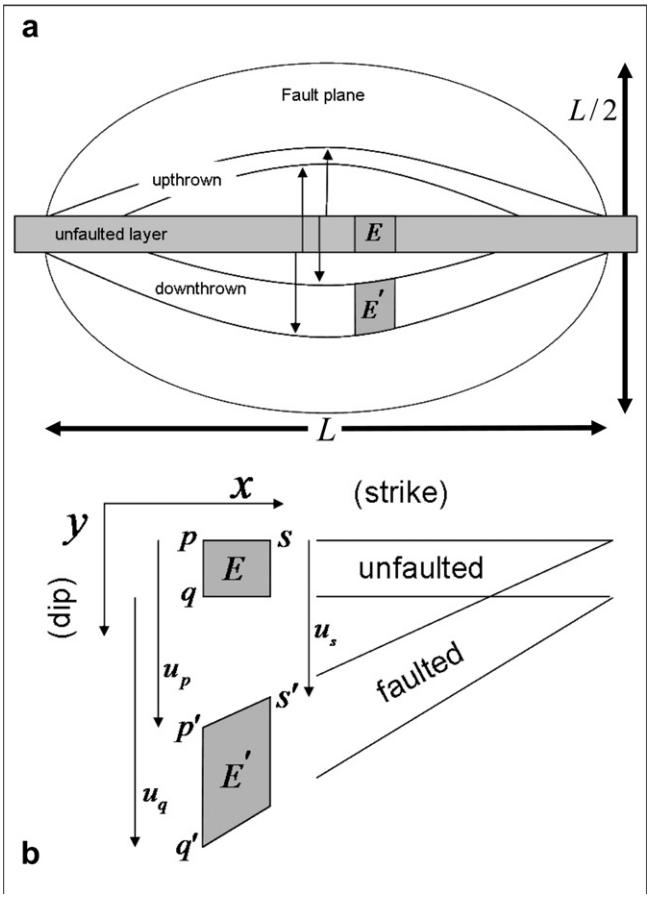

Fig. 1. (a) Schematic of an idealized fault plane (strike dimension L, dip dimension $L/2$) showing the absolute displacements from a horizontal, unfaulted layer, to the faulted, upthrown and downthrown positions. The element E in the unfaulted state is translated and strained to E'. (b) Analysis of the change in shape of the rectangular element E. x is the strike direction of the fault and y is the dip direction, u_p, u_q and u_s are absolute, dip–slip displacements.

2. Displacement and wall-rock strain

There is a simple relationship between the displacement gradient and the strain of the wall rocks in the plane parallel to the fault. Fig. 1a shows the deformation associated with the faulting of a pre-existing uniform horizontal layer (i.e. the fault is *not* a growth fault). The element, E (Fig. 1a and b), is defined by the position of the layer in the undeformed state with the top of the layer at p and the base of the layer at q (Fig. 1b). For the sake of argument we assume that displacement is in the dip direction of the fault, and that strain is partitioned equally in the two walls of the fault. The layer is then faulted such that, in the dip direction (parallel to y), p moves to p' and q moves to q'. The stretch in the dip direction is then

$$(1+e) = \frac{(u_q+q)-(u_p+p)}{(q-p)} \tag{1}$$

where e is the unit extension, u_p and u_q are the absolute displacements for one side of the fault (half the total, relative displacement). This can be re-written as

$$(1+e) = 1+\frac{1}{2}\frac{\Delta u}{\Delta y} \tag{2}$$

where the factor of 1/2 means that u refers to the total relative displacement across the fault. At the limit as Δy approaches zero

$$(1+e) = 1+\frac{1}{2}\frac{\partial u}{\partial y} \tag{3}$$

In other words the unit extension is equal to half the displacement gradient. Using an alternative formulation it is easy to show that the stretch in the upthrown layer is the reciprocal of the stretch in the downthrown layer and that the undeformed layer thickness is the average of the upthrown and downthrown thicknesses (cf. figure 1 from Barnett et al., 1987).

Referring back to Fig. 1b we can also see that, for each wall of the fault, the strain γ for shear in the dip direction is given by

$$\gamma = (u_s-u_p)/(s-p) = \frac{1}{2}\frac{\Delta u}{\Delta x} \tag{4}$$

then as Δx approaches zero

$$\gamma = \frac{1}{2}\frac{\partial u}{\partial x} \tag{5}$$

Eqs. (3) and (5) are useful results because (1) they are independent of the form of the displacement distribution, and (2) they give us a direct way to measure and represent strain from information that is almost universally available from seismic interpretations.

If we can place realistic limits on the strain values, we then have a method for distinguishing between good and bad fault interpretation that is entirely quantitative and objective.

2.1. Ideal displacement patterns for unrestricted faults

Although direct measurements of wall-rock strains is probably beyond normal field techniques, the simple fact that unrestricted faults have tip lines means that the wall rocks must be differentially strained. Eshelby (1957) and Pollard and Segall (1987) suggest the slip on a dislocation in a linear elastic solid is characterised by a semi-elliptical slip profile. In other words, a straight marker line in a wall of a fault and initially perpendicular to the slip direction will have a deformed shape of a semi-ellipse and reflects directly, the differential wall-rock strains. This type of slip profile equates to a single earthquake event. However, Nicol et al. (1996) and many others show that natural examples of unrestricted faults have approximately linear normalized profiles i.e. triangular. Furthermore Manzocchi et al. (2006) argue that this feature of geological faults seems to hold irrespective of the growth mechanism or the form of the slip profile for an individual event. This is a convenient conclusion because it means the gradient of displacement on an unrestricted fault surface is approximately constant.

2.2. Limits on displacement

Various compilations of data for D_{max}/L (D_{max} is the maximum displacement, L is the strike dimension of a fault) have been published (e.g. Bailey et al., 2005; Kim and Sanderson, 2005; Schultz et al., 2008). Although there remains debate about the exact nature of the power-law distribution of D_{max} vs L, it seems that 0.1 represents the naturally observed upper bound for all types of faults over all measured scales (Fig. 2). However, if we focus our attention on the scale range imaged on seismic data, we can refine the limit to 0.05 (Fig. 2). Then if we assume for an unrestricted fault that the displacement profile is triangular, $(1/2)\,(D_{max}/2)/(L/2) = 0.05$ places a natural limit of 0.05 on the shear strain in each wall.

Unfortunately there is no similar database for the relationship between displacement and the dip dimension of a fault. In this respect we make a further assumption that the aspect ratio of our unrestricted fault is 2 (e.g. Nicol et al., 1996), then $(1/2)\,(D_{max}/2)/(L/4) = 0.1$ represents the limit of the longitudinal strain in each wall. These suggested limits for shear and longitudinal strain are consistent with detailed measurements of coalfield fault displacement gradients by Walsh and Watterson (1989). For tip restricted or half restricted faults the displacement profile is steepened towards the tips (Nicol et al., 1996). Potentially this could increase the shear strain by a factor of two or more.

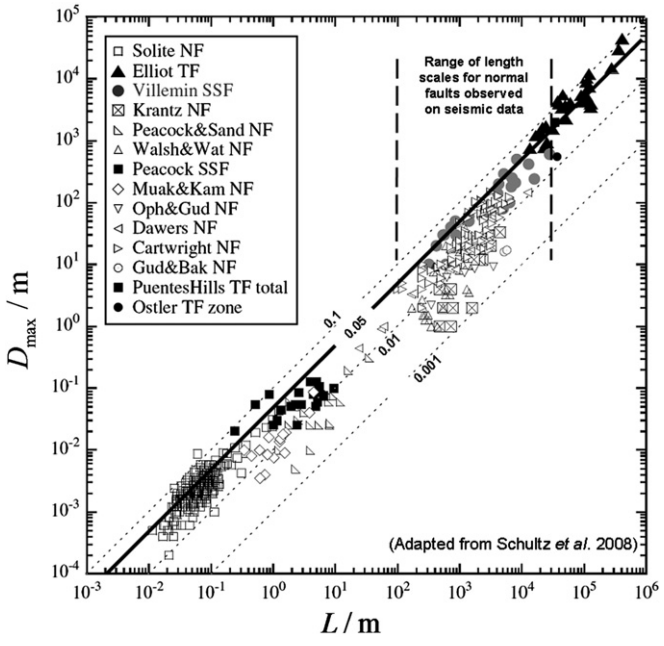

Fig. 2. Compilation of maximum displacement (D_{max}) and maximum fault length (L) adapted from Schultz et al. (2008). The data are contoured in lines of constant D_{max}/L. The 0.05 contour is our putative upper bound for D_{max}/L ratio at the range of scales of normal faults imaged on seismic data.

3. Method

All the analysis has been performed using the TrapTester software (www.badleys.co.uk/products/traptester.htm). Fault planes have been generated as triangulated meshes from the vertices of fault sticks picked on seismic sections. The horizon cutoffs at the faults are calculated from seismic interpretation of the horizons. It is rare for seismic horizon picks to tie exactly with the fault picks and therefore some extrapolation is required to make the cutoff lines. In fact we make three-dimensional surface models of both the upthrown and downthrown sides of the fault. Each of these models is extrapolated so that it extends beyond the fault in both directions and the cutoff is calculated as the intersection between the fault surface and the horizon surface model. If faults are joined at branch lines, the horizon surface model is based on the structurally coherent horizon data that is confined to the appropriate parts of the interpretation as bounded by all relevant fault planes. The quality of fit of the resulting polygons has been assessed visually and is, in all cases, a fair representation of where an expert geoscientist might draw the cutoff by hand.

Immediately prior to analysis all information for a fault plane is referred to a coordinate frame that is specific to each particular fault. We call this a natural coordinate system (NCS). The xy plane (x along strike, y down-dip) of the NCS represents a best fit plane through all the data points that define the fault plane topography. The upthrown and downthrown cutoffs form a polygon and this is the basis for the structural measurements. We measure the dip separation on a set of sweep lines (constant x) at an interval of 50 m in the x direction of the NCS. The raw measurements are interpolated on to a 50 m × 50 m grid using the multi-level B-Spline method of Lee et al. (1997). This interpolation scheme honours the raw data and produces a smoothly interpolated surface everywhere else. We calculate the strike and dip gradients of dip separation using a central difference formula.

It should be noted that the displacement gradient is measured and recorded midway between the corresponding upthrown and downthrown layers i.e. at the location in the undeformed state. However, the implied strains refer to the layers themselves i.e. the deformed state.

4. Interpretation example from South Australia

4.1. Gambier Embayment, Otway basin

The Otway Basin is a passive margin forming a large part of the Eastern Australian Rift System that resulted from the separation of Australia from Antarctica during the Late Jurassic to Late Cretaceous (Lovibond et al., 1995). Along with the rest of the Australian margin, the Otway Basin has a complex Mesozoic to present day structural history, with multiple rifting events causing principal stress/strain directions and magnitudes to change repeatedly during its development. The Gambier Embayment is a Tertiary sub-basin of the Otway Basin. It is bounded to the north and east by the Tartwaup Hinge Zone, to the west by the continental shelf and to the east it

merges (in Victoria) into the Tertiary NW–SE trending Portland Trough.

Within the Gambier Embayment the Late Cretaceous section comprises deep- to marginal-marine and deltaic sediments up to 2 km thick onshore and over 3 km offshore. The Tertiary section is up to 1000 m thick in the Gambier Embayment and is up to 2700 m in the Portland Trough. It comprises fluvial to deltaic sediments overlain by marl and limestone up to 400 m thick in the Gambier Embayment and 900 m thick in the Portland Trough (Boult, 1999; Boult and Hibburt, 2002).

4.2. Seismic data

The raw data for this study is based entirely on 2D time-migrated seismic data with approximate line spacings of 1.5 km for dip lines and 5 km for strike lines (see Fig. 3a). For the purpose of piecewise depth conversion we have used an average velocity of 3000 m s^{-1} over the entire two way time (TWT) interval. There are a number of different vintages of seismic and the quality of the reflection data is variable. For the most part fault offsets are clearly imaged in the upper part of the sections but they become less easy to interpret as the data reaches about 2000 ms. Similarly, seismic reflectors are relatively well imaged in the upper sections becoming less well imaged at depth. An example of the variability of quality is illustrated in Fig. 4.

4.3. Initial structural model

Interpretation (Essential Petroleum Resources Ltd., 2006) had been conducted using a typical industry strategy on 2D seismic panels and horizon maps and as far as we are aware, made no deliberate attempt to adhere to the basic rules of displacement continuity as outlined in the introduction to this paper. The resulting structural model comprises a set of fault planes and five horizons over a TWT range of about 2500 ms. A summary of the initial model at top reservoir level (Fig. 3b) shows an eastward shallowing structure dissected by a set of large NW–SE trending normal faults (Essential Petroleum Resources Ltd., 2006). These faults are spaced at about 2 km, they have maximum throws of about 200 ms (approximately 300 m) and maximum dip separations of the order 400 m. Throughout the discussion of these data we use dip separation as the measure of displacement in the fault plane. The top reservoir has a TWT range of the order 300 ms about an absolute TWT of 1900 ms. At this level and deeper, it becomes more challenging to tie horizons from line to line and across faults. It is therefore very important to make efficient use of the more

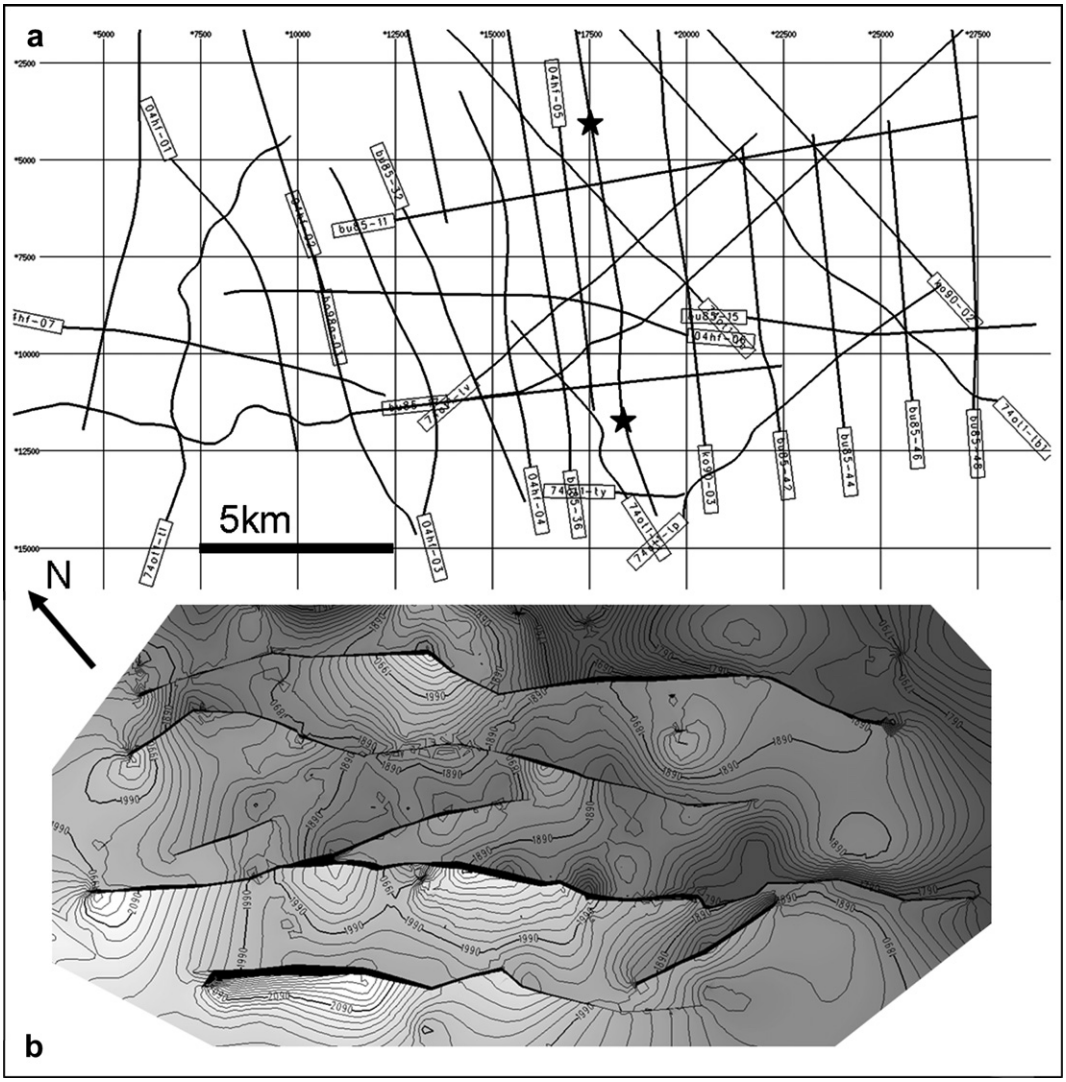

Fig. 3. (a) Base map of the 2D seismic shot lines from the Gambier Embayment, Otway Basin, South Australia. The line with the asterisks is shown in Fig. 4. (b) Prospect map at the level of top reservoir. Colour code dark to light indicates shallow to deep.

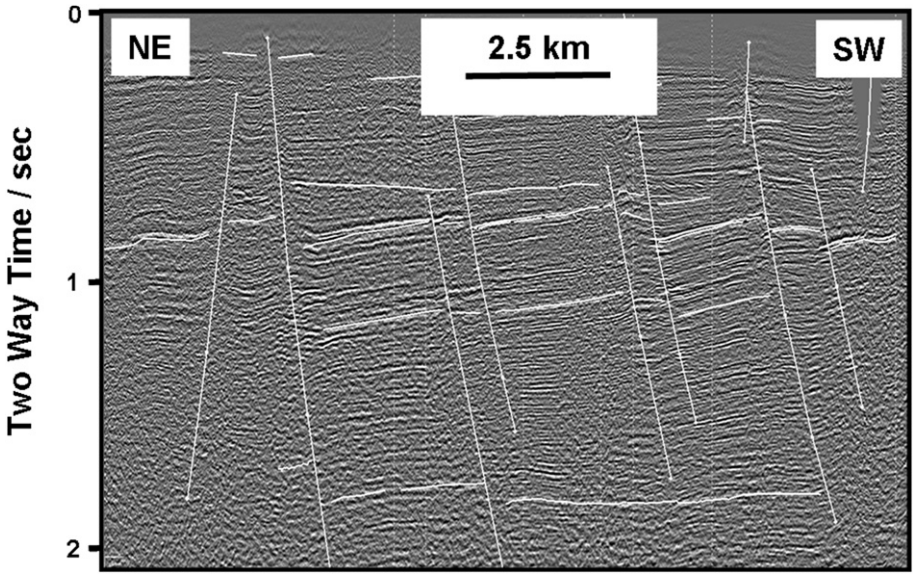

Fig. 4. Example of the 2D seismic data from line bu85-38_r9 (see Fig. 3 for location). The sub-vertical lines are fault segments, the sub-horizontal lines are horizon picks. All segments and picks are from the revised interpretation. Dashed vertical lines mark the intersection with other seismic lines.

reliable structural information above the top reservoir in order to constrain the fault model at depth. Fig. 5b–e illustrates that the fault planes themselves are picked over the full depth range. However, displacement information (from the horizon cutoffs) is limited to a relatively small area of the fault planes (approximately 50%) since not all of the five horizons are picked persistently on all lines and there were no picks at the top of the fault plane. Again, Fig. 5b–e shows the regions where the displacement information is reliable i.e. in the close vicinity of horizon picks.

Bulk measurements for the faults fall in a geologically sensible cluster with $0.1 < D_{max}/L < 0.001$. Because the maximum displacements are small relative to the interpreted fault spacing we might expect there to be minimal interference between the faults hence we might also expect simple displacement contour patterns. Notwithstanding these two observations, displacement mapping clearly shows that all of the fault planes have erratic contour patterns (Fig. 5a). They show multiple bulls-eyes (highs and lows) and exhibit both sub-vertical and sub-horizontal valleys in the displacement magnitudes. In terms of displacement gradients, hence strain, all the faults exhibit multiple lateral swings in the sign of shear strain and longitudinal strain (Fig. 5b–e). We expect shear strain to be highest at the tips, positive at the left of the strike projection and negative at the right. In fact we see the polarities inverted, locally and globally, and the high shear strains concentrated towards the centre of the faults. Equally importantly, nearly all the faults have areas where the magnitudes of the strains lie outside our bounding, acceptable threshold values (red and magenta in Fig. 5b–e). In general we take the (implied) high shear strain anomalies to indicate a location where the current fault plane should either be split in to two separate faults or where two faults join at a branch line. The anomalous (implied) longitudinal strains and associated flips in polarity usually indicate that a horizon has been picked persistently in the wrong part of the waveform on one or other side of the fault.

4.4. Revised structural model

One of us (PJB) undertook a reinterpretation of the seismic data with a view to producing (1) a model that was geologically more acceptable and (2) a model that minimized the implied strains. We picked the same five horizons with the exception of the top reservoir where, instead, we picked a reflection 200 ms above the original. (With sufficient picks the shape of the displacement distribution should be independent of the actual horizons that are chosen.) The majority of faults intersect at least three of the five horizons. In most cases the upper ends of the traces (sticks) are observed to be at zero displacement so, in addition to horizon-based displacement information, the upper tips have been explicitly assigned displacements of zero. Although all the original interpreted fault traces were reused (they received minor lateral shifts on some of the lines) our reinterpretation identified many more fault traces on each of the sections. In all we more than doubled the amount of fault information. A possible reason for the inadequacy of the original model is that the interpretation strategy was driven by picking the faults with the largest offsets and then forcing them into common-trend, lateral, correlations. In fact it is equally important to identify the fault traces with small offsets, since a fault plane can be interpreted as nearing its tip, only if it is correlated to traces with minimal displacement. In this work we have used an interpretation strategy that is both iterative and incremental inasmuch as the structure is validated as it evolves. The procedure is summarized in Boult et al. (2008).

Fig. 6 summarizes the results of the reinterpretation and we outline the major contrasts below:

(1) The new interpretation has a denser fault pattern. Unlike the original, we identify two major fault sets: one set in a NW–SE orientation (c.f. Fig. 5a), the other trending, broadly, WNW–ESE.
(2) There are no faults that transect the entire survey area. In general the new faults have smaller map dimensions than the originals. We identify isolated, *en echelon* and linked structures.
(3) The displacement contours are, largely, smooth and continuous and they are void of bulls-eyes.
(4) In general, the displacement gradients and strain patterns are also smooth and lack the erratic polarity flips that we see in Fig. 5. In particular, the implied strains are relatively low. The majority of surface area on each fault has strain values well below our upper bounds.

(5) Values of longitudinal strains mostly lie in the range $-0.1 < e < 0.1$ and they are tightly clustered around smaller values. The signs are uniformly positive in the upper parts of the fault and negative at depth. However, on several of the faults we see persistent bands of high implied strain that lie outside our upper limit (red colours in Fig. 6b and c). Initially this appears to put the interpretation in question but in fact, the top horizon is picked above an unconformity. This gives the effect of anomalously high displacement gradients and we take these high values to indicate that the faults were at least partially active prior to the unconformity.
(6) The two fault trends (above) can also be distinguished on the basis of the displacement and longitudinal strain patterns. The NW–SE set displays a symmetry that we associate with displacement dying out towards both an upper and lower tip while the WNW–ENE set has displacement increasing downwards.
(7) The shear strain patterns show an obvious symmetry with low values in the central part of the fault, increasing to maximum values at each lateral tip.
(8) To a large degree the shear strain maps conform to our notion of maximum strain. The polarities are mostly consistent and the extents of regions where the strains are beyond our limits of $\gamma = 0.05$ are confined to the fault tip regions. This increase in gradient and strain towards the tips is likely to be a consequence of interference between two or more faults.

5. Discussion and conclusions

We have shown that measurement of displacement and mapping of displacement gradients leads to the notion of limits to the wall-rock strain either side of a fault. Applying these limits allows us to make objective judgements about the validity of fault interpretation from seismic data and thus reduces the uncertainty inherent in the interpretation process. In practice it is the bounding values that are important and it is of little consequence whether the actual metric that is used is the displacement gradient or the strain. The displacement gradient is, of course, the measured quantity but its meaning is slightly less tangible than strain. Strain is a quantity that is more commonly used in the literature and more likely to be linked, at least intuitively, to other phenomenon. For example, one might predict there to be a correlation between wall-rock strain and the degree of fracture damage in the close vicinity of a fault.

The brief and simple analysis (Eqs. (3) and (5)) is based on dip–slip relative motion. Therefore its application is most suitable for unrestricted, normal or reverse faults. However, dip separation is always a minimum estimate of the true slip magnitude; for dip–slip faults it is exact but for oblique slip faults it is less than the true slip. Similarly our estimate of both the longitudinal strain and the shear strain will underestimate the values in the true slip direction. We would suggest that for minor obliquity the dip slip thresholds may still be usefully applied but it would be more accurate if either (1) the dip slip values were to be corrected for the rake of the slip vector or (2) the offsets were to be measured along the slip direction. But precise slip direction is almost always impossible to determine from seismic reflection data.

Given the generality of approximately triangular displacement profiles, we believe the upper limit we place on shear strain of $\gamma = 0.05$ for isolated faults at the seismic scale is reasonably robust since it is based on a large collection of D_{max}/L data. As we have already discussed, the limit of $D_{max}/L = 0.05$ seems to hold over the scale range observed on seismic reflection data. However, we should note that other workers show that small faults (up to $L = 5$ m) in incompletely lithified sand have D_{max}/L bounded at 0.1. The contrast in mechanical properties with completely lithified sandstone in elasto-plastic models of fault propagation can explain such increases (Wibberley et al., 1999). Similarly, at the upper end of the scale thrust faults also seem to be bounded by $D_{max}/L = 0.1$ (see Fig. 2), but this may be due to other processes such as tip propagation blocking by basalt layers (Puentes Hills), or ductile deformation mechanisms accommodating along-strike decollement strains (Rocky Mountains thrusts). Although there are issues involving sampling of the principal axis of a fault, the strike dimension and maximum offset are relatively straightforward to measure. The main source of uncertainty is whether or not the faults in the compilation (Fig. 2) are truly isolated. If the highest D_{max}/L values are due to faults that are horizontally restricted, then our estimate of maximum shear strain will be too high. We should also note that in all our natural examples described here the shear strain gradient is lower at the centre of the faults than at the tips and that the gradient is highest between the fault centre and the tips i.e. the pattern is actually more of a bell shape than linear. Moreover, in the vicinity of overlapping tips, we record higher shear strains than the upper limit we expect for isolated faults. This is consistent with other natural examples (Nicol et al., 1996) and with the effect of mechanical interaction between two faults. Relative to an unrestricted fault, the shear strain, where faults overstep, increases with size of overlap, dip dimension and decreasing distance between the faults (Willemse, 1997). Again, these high strain zones may give an indication of sub-seismic scale fracturing and thus have some impact on the local fluid flow behaviour.

Maximum allowable longitudinal strain in the dip slip direction is less robust. Schultz and Fossen (2002) argue that the displacement scales not only with length but with aspect ratio and that the highest D_{max}/L corresponds to the smallest aspect ratios. Soliva et al. (2005) report a similar phenomenon that for a given constant fault height, D_{max}/L decreases with length. Both of these studies refer to outcrop scale observations where the structures are confined to single layers. Beyond outcrop scale the dip dimension of faults is, by comparison with the strike dimension, more difficult to constrain. For example on seismic reflection data it is common for the upper tips to be truncated at unconformities and/or the lower tips to be not imaged clearly. Consequently there is little in the way of published data that incorporates D_{max}, L and aspect ratio at the scale of seismically imaged faults. Nicol et al. (1996) show that the aspect ratios of unrestricted faults, over the scale range of 10s of metres to 10s of kilometers, lie between 1 and 3 but unfortunately they provide no information on the maximum displacement for the same faults. In setting our upper limit we have tried to embrace both of these sets of observations, so a maximum longitudinal strain of $e = 0.1$ is based on $D_{max}/L = 0.05$ and the ellipticity of a fault being a maximum of 2:1.

Our upper limit of dip-direction longitudinal strain leads to a maximum layer thickness ratio of approximately 1.2 for corresponding layers either side of the fault. Note that we are describing fault-related strain of pre-faulting layers, not thickness changes in syn-faulting layers (i.e. growth sequences). Increasing the aspect ratio of the ellipse and maintaining the same displacement and strike dimension (in contrast to Soliva et al. (2005), above) dramatically increases the implied longitudinal strain. For example an ellipticity of 3:1 implies a maximum longitudinal strain of $e = 0.15$ and differential thicknesses of 1.35. In our experience apparent strains of this magnitude are always associated with sedimentary growth or they are found near the tops of faults that have been truncated by unconformities. In either case they are not real strains. On the other hand choosing an aspect ratio of unity reduces the upper limit by a factor of two to $e = 0.05$. We believe

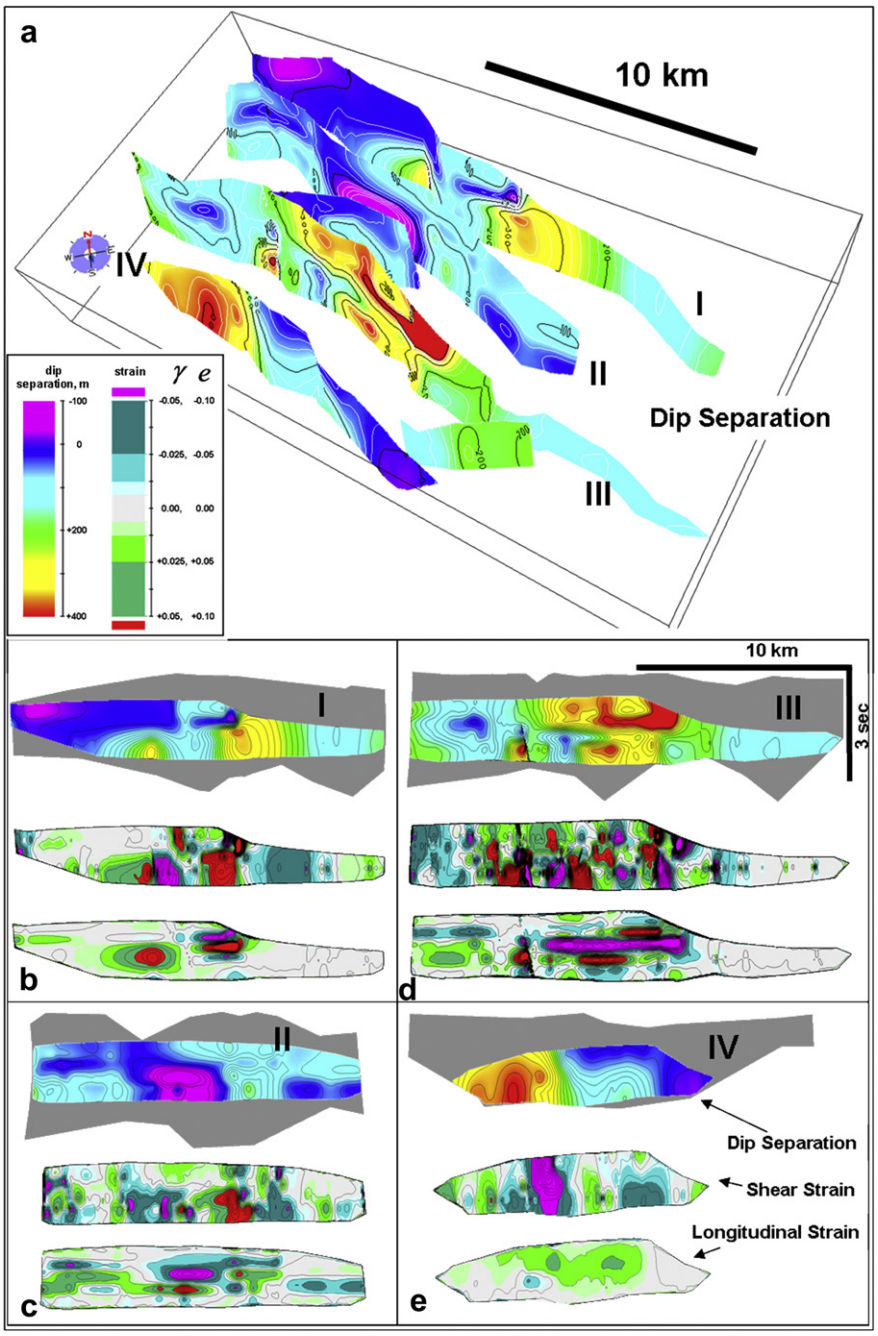

Fig. 5. (a) Perspective view of the faults from the original interpretation, colour coded and contoured in dip separation. The fault surfaces are displayed only where the displacement information is present. Details of faults I, II, III, and IV are shown in strike projection in b through e. In each panel (b–e) the top image shows the entire fault surface (grey) and the region where displacement information is present is colour coded in dip separation. Beneath is the map of shear strain, beneath that is the map of longitudinal strain. In the legend the strains can be converted to displacement gradient by multiplying by two.

that the routine examination of longitudinal strain should provide a valuable quality control metric but we also suggest that the published database for D_{max}, L and aspect ratio needs to be enhanced.

All our analysis and discussion is based on upper limits to strain. It is also possible, from the point of view of 2D seismic interpretation, for faults to be over-correlated laterally with large fault strike lengths but only very small displacements. It seems that this type of error is more difficult to quantify in terms of strain limits since the range of known D_{max}/L implies that strains could easily be at least 100 times less than our upper bounds.

There remains the problem of anomalous implied strains in the walls of faults which, in all other respects, have been interpreted using this minimum strain approach. Depending on scale and quality of the seismic data it is always possible that relatively small structures are missed from the interpretation. In which case, these anomalies may be the best indication of additional, real, structure. Although we strongly caution against the "invention" of structure it may be that such indirectly observed features could be incorporated into end member structural models. These would have particular significance if the three-dimensional structural model is to be used for fluid flow simulation.

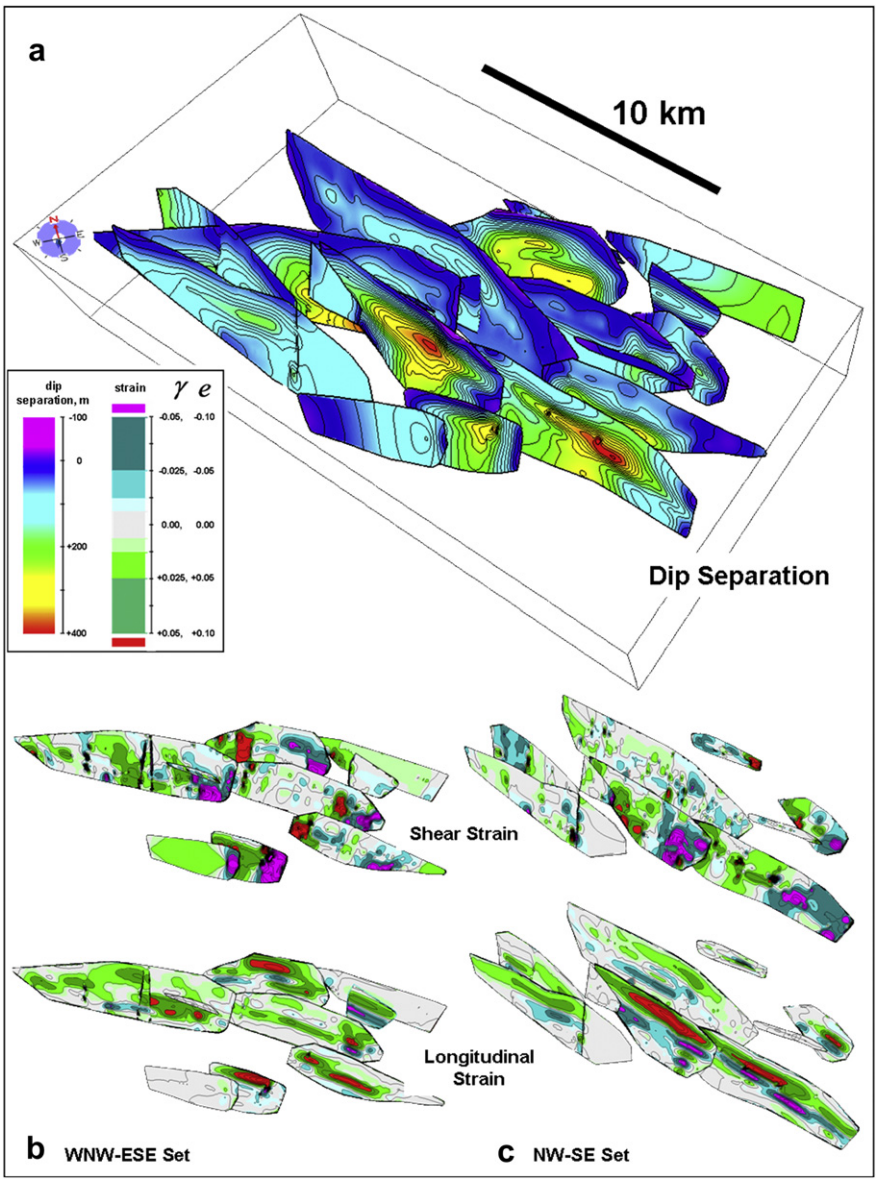

Fig. 6. (a) Perspective view of faults from the reinterpretation, colour coded and contoured in dip separation. (b) Shear strain (upper) and longitudinal strain (lower) maps of the WNW–ESE fault set. (c) Shear strain (upper) and longitudinal strain (lower) maps of the NW–SE fault set.

5.1. Conclusions

(1) The problem of validating fault interpretation from seismic data can be addressed using displacement and strain analysis.
(2) There is a simple relationship between instantaneous displacement gradients and wall-rock shear and longitudinal strains.
(3) For unrestricted faults, reasonable natural upper limits to the magnitudes of shear strain and longitudinal strain in the dip slip direction are 0.05 and 0.1 respectively.
(4) Faults with strains that lie above these bounds are unlikely to be correlated correctly.
(5) Fault interpretations that minimize the wall-rock strains provide the most feasible geological solution.

Acknowledgements

We would like to thank the many colleagues at Badley Geoscience Ltd and the Fault Analysis Group whose ideas have helped to shape this work. The manuscript has benefited from editing by Chris Wibberley and the careful and constructive reviews of Matt Pachell and one anonymous reviewer.

References

Bailey, W.R., Walsh, J.J., Manzocchi, T., 2005. Fault populations, strain distribution and basement fault reactivation in the East Pennines Coalfield, UK. Journal of Structural Geology 27, 913–928.
Barnett, J.A., Mortimer, J., Rippon, J.H., Walsh, J.J., Watterson, J., 1987. Displacement geometry in the volume containing a single normal fault. American Association of Petroleum Geologists Bulletin 71, 925–937.
Boult, P.J., 1999. Maturity Modelling of the Casterton Formation and Killara Coals in PEP 111 and PEP 101. Boral Energy Resources Ltd., Otway Basin, Victoria. Unpublished report.
Boult, P.J., Hibburt, J.E. (Eds.), 2002. The Petroleum Geology of South Australia. Vol. 1: Otway BasinPetroleum Geology of South Australia Series, second ed., vol. 1. Department of Primary Industries and Resources, South Australia.
Boult, P, Freeman, B., Yielding, G., Menpes, S., Diekman, L.J., 2008. A minimum-strain approach to reducing the structural uncertainty in poor 2D seismic data, Gambier Embayment, Otway Basin, Australia. In: Proceedings of the Third Eastern Australasian Basins Symposium, Sydney, September 14th–17th.

Bouvier, J.D., Kaars-Sijpesteijn, C.H., Kluesner, D.F., Onyejekwe, C.C., Van der Pal, R.C., 1989. Three-dimensional seismic interpretation and fault sealing investigations, Nun River Field, Nigeria. American Association of Petroleum Geologists Bulletin 73, 1397–1414.

Chapman, T.J., Meneilly, A.W., 1991. The displacement patterns associated with a reverse-reactivated, normal growth fault. In: Roberts, A.M., Yielding, G., Freeman, B. (Eds.), The Geometry of Normal Faults. Geological Society of London, Special Publication, vol. 56, pp. 183–191.

Eshelby, J.D., 1957. The determination of the elastic field of an ellipsoidal inclusion and related problems. Proceedings of the Royal Society of London, Series A 241, 376–396.

Essential Petroleum Resources Ltd., 2006. Internal Presentation to the PEL 72 Joint Venture Technical Committee.

Freeman, B., Badley, M.E., Yielding, G., 1990. Fault correlation during seismic interpretation. First Break 8, 87–95.

Kim, Y.-S., Sanderson, D.J., 2005. The relationship between displacement and length of faults: a review. Earth-Science Reviews 68, 317–334.

Lee, S., Wolberg, G., Shin, S.Y., 1997. Scattered data interpolation with multilevel B-splines. IEEE Transactions on Visualization and Computer Graphics 3, 228–244.

Lovibond, R., Suttill, R.J., Skinner, J.E., Aburas, A.N., 1995. The hydrocarbon potential of the Penola Trough, Otway Basin. APEA Journal 35, 358–371.

Manzocchi, T., Walsh, J.J., Nicol, A., 2006. Displacement accumulation from earthquakes on isolated normal faults. Journal of Structural Geology 28, 1685–1693.

Needham, D.T., Yielding, G., Freeman, B., 1996. Analysis of fault geometry and displacement patterns. In: Buchanan, P.G., Nieuwland, D.A. (Eds.), Modern Developments in Structural Interpretation, Validation and Modelling. Geological Society of London, Special Publication, vol. 99, pp. 189–199.

Nicol, A., Watterson, J., Walsh, J.J., Childs, C., 1996. The shapes, major axis orientations and displacement patterns of fault surfaces. Journal of Structural Geology 18, 235–248.

Pollard, D.D., Segall, P., 1987. Theoretical displacements and stresses near fractures in rock: with applications to faults, joints, veins, dikes, and solution surfaces. In: Atkinson, B.K. (Ed.), Fracture Mechanics of Rock. Academic Press, London, pp. 277–349.

Rippon, J.H., 1985. Contoured patterns of the throw and hade of normal faults in the Coal Measures (Westphalian) of north-east Derbyshire. Proceedings of the Yorkshire Geological Society 45, 147–161.

Schultz, R.A., Soliva, R., Fossen, H., Okubo, C.H., Reeves, D.M., 2008. Dependence of displacement–length scaling relations for fractures and deformation bands on the volumetric changes across them. Journal of Structural Geology 30, 1405–1411.

Schultz, R.A., Fossen, H., 2002. Displacement–length scaling in three dimensions: the importance of aspect ratio and application to deformation bands. Journal of Structural Geology 24, 1389–1411.

Soliva, R., Schultz, R.A., Benedicto, A., 2005. Three-dimensional displacement–length scaling and maximum dimension of normal faults in layered rocks. Geophysical Research Letters 32, L16302. doi:10.1029/2005GL023007.

Walsh, J.J., Watterson, J., 1989. Displacement gradients on fault surfaces. Journal of Structural Geology 11, 307–316.

Wibberley, C.A.J., Petit, J.-P., Rives, T., 1999. Mechanics of high displacement gradient faulting prior to lithification. Journal of Structural Geology 21, 251–257.

Willemse, E.M.J., 1997. Segmented normal faults: correspondence between three-dimensional mechanical models and field data. Journal of Geophysical Research 102 (B1), 675–692.